ACS APPLIED MATERIALS & INTERFACES

Research Article

www.acsami.org

Defect Structure Analysis of Heterointerface between Pt and CeO_x Promoter on Pt Electro-Catalyst

Keisuke Fugane,[†,‡,§] Toshiyuki Mori,*[,†,‡] Pengfei Yan,[†] Takuya Masuda,[†,#] Shunya Yamamoto,[∥] Fei Ye,[⊥] Hideki Yoshikawa,[#] Graeme Auchterlonie,[▽] and John Drennan[▽]

[†]Global Research Center for Environmental and Energy Based on Nanomaterials Science (GREEN), National Institute for Materials Science (NIMS), 1-1 Namiki, Tsukuba, Ibaraki 305-0044, Japan

[‡]Graduate School of Chemical Science and Engineering, Hokkaido University, Kita 13, Nishi 8, Kita-ku, Sapporo, Hokkaido 060-8628, Japan

[§]Corporation Technical Research Institute, Hitachi Zosen, 2-11, Funamachi 2-chome Taisho-ku, Osaka 551-0022, Japan

[∥]Quantum Beam Science Directorate, Japan Atomic Energy Agency (JAEA), 1233 Watanuki, Takasaki, Gunma 370-1292, Japan

[⊥]School of Materials Science and Engineering, Dalian University of Technology, 2 Linggong Road, Dalian, Liaoning 116024, China

[#]Nano Characterization Unit, National Institute for Materials Science (NIMS), 1-2-1 Sengen, Tsukuba, Ibaraki 305-0047, Japan

[▽]Centre for Microscopy and Microanalysis, The University of Queensland, St. Lucia, Queensland 4072, Australia

S *Supporting Information*

ABSTRACT: Pt−CeO_x/C ($1.5 \leq x \leq 2$) electro-catalyst is one of the most promising cathode materials for use in polymer membrane electrolyte fuel cells. To clarify the microstructure of Pt−CeO_x heterointerface, we prepared Pt-loaded CeO_x thin film on conductive $SrTiO_3$ single crystal substrate by using a stepwise process of pulse laser deposition method for the preparation of epitaxial growth CeO_x film followed by an impregnation method which loaded the Pt particles on the CeO_x film. The electrochemistry observed for the Pt-loaded CeO_x thin film on the conductive single crystal substrate was examined by using cyclic voltammetry in 0.5 M H_2SO_4 aqueous solution, and a cross-sectional image of the aforementioned Pt−CeO_x thin film electrode was observed using a transmission electron microscope. The electrochemistry observed for Pt−CeO_x thin film electrode clearly showed the promotion effect of CeO_x. Also, the microanalysis indicated that unique, large clusters that consisted of C-type rare-earth-like structures were formed in the Pt−CeO_x interface by a strong interaction between Pt and CeO_x. The present combination analysis of the electrochemistry, microanalysis, and atomistic simulation indicates that the large clusters (i.e., 12 (Pt_{Ce}''−$Vo^{\bullet\bullet}$) + 2 (Pt_{Ce}''−$2Vo^{\bullet\bullet}$−$2Ce_{Ce}'$)) that were formed into the Pt−CeO_x interface promoted the charge transfer between Pt surface and CeO_x, suggesting that the oxygen reduction reaction activity on Pt can be maximized by fabrication of C-type rare-earth-like structure that consists of the aforementioned large clusters in the Pt−CeO_x interfaces.

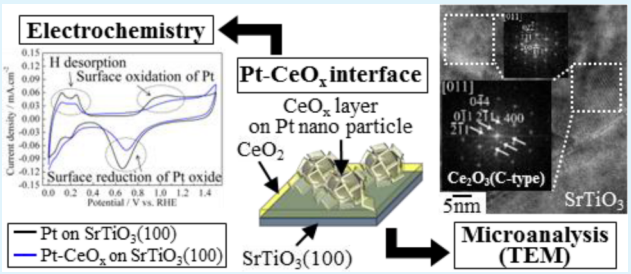

KEYWORDS: *Pt−CeO_x interface, microanalysis, atomistic simulation, promotion effect of CeO_x, Pt cathode, fuel cell*

1. INTRODUCTION

Fuel cells are a clean and efficient power source for generating electricity by using hydrogen and oxygen.[1−3] One strategy to reduce the price of the fuel cell device is to reduce the Pt content of the electrode materials. However, this must be achieved with minimal loss in the performance of the electro-catalyst.

Recently, the non-platinum cathodes such as carbon-based materials (i.e., N-doped carbon nanotube array,[4] N-doped graphene,[5] graphene-based carbon−nitride nanosheet,[6] S-doped graphene,[7] and graphene oxide[8]) have been proposed for polymer electrolyte fuel cell (PEFC) applications. However, the most suitable cathode in PEFCs is still platinum (Pt) nanoparticles loaded onto conductive carbons as a result of their reliable oxygen reduction reaction (ORR) activity and their stability under many operating conditions. On the other hand, Pt cathode materials still have the problem of a large overpotential loss of the ORR as a consequence of the slow kinetics at the surface of the Pt particles in the potential range from 0.75 to 1.0 V (vs reversible hydrogen electrode, RHE). As a result, lowering the overpotential loss on the Pt surfaces is a key issue for the future development of PEFCs.

An effective way to solve this challenge is to modify the Pt/C electro-catalyst by using an oxide promoter such as WO_3,[9] TiO_2,[9] NbO_2,[10] SnO_2,[11] or CeO_2.[12−18] Among these candidate materials, CeO_x ($1.5 \leq x \leq 2$) has received considerable

Received: November 6, 2014
Accepted: January 8, 2015
Published: January 8, 2015

DOI: 10.1021/am507754w
ACS Appl. Mater. Interfaces 2015, 7, 2698−2707

attention as a unique oxide promoter with properties based on electrochemical redox reaction of CeO_x ($Ce^{3+} \leftrightarrow Ce^{4+}$) at room temperature. Masuda et al. examined the interface reaction on Pt with Pt−CeO_x interface by using in situ X-ray absorption fine structure (XAFS) analysis method.[19] They suggested that the surface electrochemical oxidation of Pt can be effectively suppressed by using the electrochemical redox reaction of CeO_x in the Pt−CeO_x interface, and the ORR activity can be enhanced by using the aforementioned unique CeO_x property at room temperature. The long-term stability of the Pt−CeO_x interface was examined by using a long cyclic voltammetry (CV) test, up to 1000 cycles in H_2SO_4 aqueous solution. When the applied potential was varied from 0 to 1.5 V (vs RHE), the ORR activity observed for Pt−CeO_x/C slightly decreased during 1000 cycles test and some amount of CeO_x layer peeled off from Pt surface.[16] In contrast, the long CV test up to 1000 cycle sweeps by using potential ranging from 0 to 1.0 V (vs RHE) shows quite stable and high ORR performance in H_2SO_4 aqueous solution. Also, the CeO_x layer on Pt after long CV test was almost same to the as-prepared sample.[17] This result suggests that Pt−CeO_x interface has high stability in the potenatial cycle from 0 to 1.0 V (vs RHE). It indicates that the Pt−CeO_x interface is useful for the development of PEFC devices in which cell potential is from 0 to 1.0 V. In addition, Ou et al. observed the Pt−CeO_x interface structure on Pt particle by using high resolution TEM and they compared the key defect structure of Pt−CeO_x interface before and after electrochemical pretreatment process.[20,21] On the basis of their careful observation, they suggested the Pt cation dissolution in the CeO_x matrix of Pt−CeO_x interface by using analytical TEM. In related work in terms of strong Pt and CeO_x interaction, Bruix et al. showed the large electronic perturbations for Pt in contact with CeO_x and improved catalytic activities on well-defined catalytic surface in water−gas shift (WGS) reaction. In addition, they performed discrete Fourier transform calculations to consider the water molecule dissociation process with charge transfer on small Pt clusters that interact with CeO_x.[22] They demonstrated the electronic properties of the Pt−CeO_x interface showing important perturbations in the density-of-states of the metal near its Fermi level plus charge transfer. Suchorski et al. fabricated well-defined CeO_x/Pt(111) model catalyst and monitored CO oxidation reaction.[23] In their work, both of the redox behavior of CeO_x in Pt−CeO_x catalyst and improvement of CO oxidation activity on Pt were clearly demonstrated.[23]

However, the Pt−CeO_x interface structure on Pt particle cathode after the electrochemical pretreatment process has not been fully explained yet as the result of limitation of interface area formed between nanosized Pt and CeO_x particles. Also, the relationship between the ORR property on Pt in contact with CeO_x and Pt−CeO_x interface structure has not been considered yet in the literature, though the influence of Pt−CeO_x interaction on the catalytic activity observed for Pt-loaded CeO_x in both of the WGS and CO oxidation reactions was examined.

To maximize the unique function of CeO_x promoter on Pt and develop Pt less cathodes with high ORR activity, we required more detailed characterization of Pt−CeO_x interface structure, which was widely formed on thin film electrode, and thus used several microanalysis techniques (i.e., XPS, TEM and so on). In addition, in an attempt to interpret the TEM observations, we have undertaken a series of atomistic simulations based on the microanalysis results, and these are presented in the Discussion section. On the basis of results of the ORR activity measurement, microanalysis and atomistic simulation, the key defect Pt−CeO_x interface structure, which would influence a promoting effect of CeO_x for improvement of ORR activity on Pt, is highlighted.

2. EXPERIMENTAL SECTION

2.1. Sample Preparation. Pt−CeO_x/C particle cathode was prepared in a stepwise process. The pure CeO_x powder was synthesized by a hot ammonium carbonate precipitation method. The preparation detail of pure CeO_x was described in a previously published paper.[16] Because CeO_x surface has basic nature and easily adsorbs H_2O molecules in high moisture atmosphere, the moisture control at low level for the mixture of platinum chloride salts and nanosized CeO_x particles is required to minimize the agglomeration of nanosized Pt on CeO_x nanoparticles. To impregnate fine Pt particles on the prepared CeO_x nanoparticles, $H_2PtCl_6{\cdot}6H_2O$ powder was dissolved in ethanol, which was dehydrated in advance by molecular sieve. This mixing process was performed in a glovebox where the moisture level was kept below 10 ppm. The pure CeO_x powder which was prepared in advance was dispersed in the H_2PtCl_6 ethanol solution and dried in the glovebox. The dried mixture was calcined at 400 °C for 1 h in a 10% H_2/He mixed gas flow. Then, the prepared Pt−CeO_x was mixed with carbon black (C; Vulcan XC-72R, Cabot Co.) and dispersed in C_2H_5OH and dried in a N_2 gas flow.

Pt−CeO_x thin film cathode was prepared by using combination of pulsed laser deposition (PLD) and impregnation methods. The experimental setup used for PLD has been described in detail elsewhere.[24] The laser ablation was carried out on CeO_2 target (purity of CeO_2 powder, 99.9%; disc size, 50 mm in diameter and 5 mm thickness; Furuuchi Chemical Co., Ltd.). CeO_x film was deposited on the conductive single crystal substrate by using PLD method. The commercially available epi-polished $SrTiO_3$ single crystal doped with Nb (Shinkosha Co., Ltd.; Nb content, 0.5 wt %; specific resistance, 3−7 × 10^{-3} Ω·cm) in which crystal orientation is (100) was used as the conductive single crystal substrate. The size of substrate is 10 × 10 × 0.5 mm.

PLD was performed by the second harmonic Q-switched Nd/YAG laser with the wavelength of 532 nm, 8 ns in pulse width and 5 Hz in frequency. During the deposition, the laser was focused onto the continuous rotating CeO_2 target (i.e., 5 rpm). The substrate was separated from the target by approximately 5 cm. In the present PLD process, the substrate temperature was set at 570 °C under residual O_2 gas pressure of 5.3 Pa. The deposition time was 30 min with the laser energy of 30 mJ $pulse^{-1}$. The estimated thickness of CeO_x film on Nb-doped $SrTiO_3$ (100) single crystal substrate (Nb-STO SCS) was approximately 50 nm (in terms of determination method of film thickness, see the Characterization section). After the PLD process, the CeO_x film was annealed at 1000 °C for 1 h to improve its crystallinity.

To impregnate fine Pt particles on both Nb-STO SCS and the prepared CeO_2 thin film, which was deposited on Nb-STO SCS, $H_2PtCl_6{\cdot}6H_2O$ powder was dissolved in ethanol under the glovebox conditions where the moisture level was kept below 10 ppm. To fabricate the electrode layer (area, 19.6 mm^2), which contains 2 μg of Pt on the Nb-STO SCS, a predetermined amount of H_2PtCl_6 ethanol solution was dispersed on both Nb-STO SCS and CeO_x thin film deposited on the substrate. After drying in the globe box, the aforementioned H_2PtCl_6-loaded CeO_x thin film on substrate and the H_2PtCl_6 loaded on the substrate were calcined at 400 °C for 1 h in a 10% H_2/He gas flow.

2.2. Electrochemical Properties Measurement. The cathode properties of Pt−CeO_x/C particle and Pt−CeO_x thin film were examined in 0.5 M H_2SO_4 aqueous solution in the potential range from 0.95 to 0 V (vs Ag/AgCl) by using a potentiostat/galvanostat (HSV100, Hokuto Denko Corp., Japan). The water was purified using a reverse osmosis/electro-deionization system (MILLPORE, Elix Advantage, Japan), and ultrapure reagent-grade H_2SO_4 (Kishida

DOI: 10.1021/am507754w
ACS Appl. Mater. Interfaces 2015, 7, 2698−2707

Chemicals Corp., Japan) was used for preparation of electrolyte solution.

The electrochemical measurements were carried out by using a standard three-electrode glass cell after the conditioning process at 28 °C. Pt foil and Ag/AgCl were used as counter and reference electrodes, respectively.

To compare the electrochemistry observed for the two types of electrodes, particle cathode and thin film cathode, the particle cathode samples were prepared from a suspension of the cathode materials (2 mg ml^{-1}) in C_2H_5OH solution. The suspension was spread onto the surface of a glassy carbon (area, 38.5 mm^2) electrode using a micropipette. The amount of the cathode materials on the electrode was 5 μL.

The conditioning process of the cathode surface, which we refer to as electrochemical pretreatment, was necessary to obtain active and stable electrochemical performance. The standard electrochemical pretreatment in the present work was performed by means of 30 cycle sweeps in N_2-saturated 0.5 M H_2SO_4 aqueous solution using the potential range from −0.2 to 1.3 V (vs Ag/AgCl). After the steady state condition was observed, the surface oxidation level of Pt was estimated from the observed charge ratio between oxidation charge (Q_{OX}) and hydrogen adsorption charge (Q_H). The geometric surface area which was calculated by using Levich's equation (sweep rate: 10 mV sec^{-1}) was used for the calculation of the current density. For the measurement of the stable electrochemistry on Pt-loaded CeO_x thin film electrode, the ohmic contact between the Nb-STO SCS and working electrode (Au) was achieved using gallium indium (GaIn) alloy paste. The measured potentials were converted to the RHE scale.

2.3. Characterization. The Rutherford backscattering spectrometry (RBS)/channeling analysis was performed to characterize the epitaxy of the thin film by employing 2.0 MeV He^+ ions. The backscattered particles were detected at 165° with a surface barrier detector. Samples were mounted on a three-axis goniometer to pattern the planar channeling and the axial channeling in the angular coordinate. Also, the orientation of the heteroepitaxial thin film was examined by using X-ray diffraction measurement (Ultima+, Rigaku Corp., Japan). The X-ray source was operated at 40 kV and 40 mA for Cu Kα radiation (λ = 0.154 nm). The thickness of thin film was determined by measurement of step height difference between deposited and undeposited areas on the substrate. The thickness was determined by using surface profiler (DEKTAK3ST, Veeco Company, Japan).

The surface chemical states of Pt-loaded Nb-STO SCS, CeO_x thin film on Nb-STO SCS, and Pt-loaded CeO_x thin film on Nb-STO SCS were analyzed by photoelectron spectroscopy (PES). To characterize the surface composition, we performed PES at different excitation energies. Because the probing depth of hard X-ray PES (HXPS) is much deeper than that of soft X-ray PES (SXPS), the average chemical states of deep surface area and top surface of the electrodes on the conductive single crystal substrate can be compared by using the two kinds of XPS experimentations (i.e., HXPS and SXPS). The HXPS experiments were performed at the undulator beamline BL15XU of the synchrotron facility, SPring-8. X-rays monochromatized at 5946 eV (inelastic mean free path of photoelectrons from Ce 3d of CeO_2 is 7.1 nm) using a Si111 double-crystal monochromator and a Si333 post channel-cut crystal, were focused onto specimens mounted in an analysis chamber attached to a high-resolution electron analyzer (VG Scienta R4000-10 kV). The SXPS spectra were observed using a standard laboratory Al Kα X-ray source ($h\nu$ = 1486.6 eV, inelastic mean free path of photoelectrons from Ce 3d of CeO_2 is 2.3 nm). The SXPS experiments were performed using Thermo Scientific Theta Probe. The binding energy of Pt 4f and Ce 3d core level peaks were corrected using the binding energy of C 1s core level peak as 284.5 eV. The peak separation analysis was performed using software UNIFIT2009 (Leipzig University, Germany). The cross-sectional image of Pt-loaded CeO_x thin film which was deposited on Nb-STO SCS was investigated by transmission electron microscopy (TEM), using a JEOL JEM-2000EX electron microscope operating at 200 kV. The fast Fourier transforms and inverse fast Fourier transforms patterns taken from the cross-sectional image were characterized for identification of the crystal structure of Pt−CeO_x heterointerface of thin film electrode.

2.4. Atomistic Simulation. To study the defect cluster structure in the heterointerface of the Pt-loaded CeO_x thin film electrode, we performed atomistic simulation. The lattice energy is the sum of long-range Coulombic interactions and short-range interactions described by parametrized pair potentials, S_{ij}. The short-range interactions are modeled using a Buckingham potential form $S_{ij} = A \exp(-r_{ij}/\rho) - Cr_{ij}^{-6}$, where A, ρ, and C are adjustable parameters. The values of these parameters are listed in Table 1.[25] The short-range interactions are set to zero beyond a cutoff of 20 Å. The effect of ionic polarizability of O^{2-} and Ce^{4+} ions is included via the shell model.[25] In this model, the ions are comprised of a massive core with charge Xlel and a mass less shell with charge Ylel. The overall charge state of each ion is equal to (X + Y)lel. The core and shell are connected by an isotropic harmonic spring of force constant k. These shell parameters are listed in Table 2.[25] To predict how a lattice accommodates defects, we used the Mott−Littleton two-region approach for the simulation of the defect formation energy, which is coded in the General Utility Lattice Program (GULP).[26] In this approach, the lattice for energy minimization is partitioned into two regions: a spherical inner region I, at the center of which the defects are introduced, and an outer region II, which extends to infinity. To ensure a smooth transition between regions I and II, we introduced interfacial region IIa. In the present work, we used an inner region I with a radius of 3.0 a_0 (a_0 is 5.411 Å, which is the lattice constant of CeO_2) and an interfacial region IIa with a radius of 6.0a_0. To calculate the intrinsic defect energy, we applied the Mott−Littleton two-region method. Also, the binding energy ΔE_b is calculated to investigate the preference and stability of defect clusters. It is described as $\Delta E_b = \sum E_{isolated} - E_{cluster}$, where $\sum E_{isolated}$ is the sum of the defect energy for all individual components and $E_{cluster}$ is the entire defect energy of this cluster. Note that the calculated binding energy has to be positive value when the assumed clusters in this modeling are stable.

Table 1. Short-Range Potential Parameters

species	A (eV)	ρ (Å)	C (eV Å^6)
$Ce^{4+}-O^{2-}$	1809.68	0.3547	20.40
$Ce^{3+}-O^{2-}$	2010.18	0.3449	23.11
$Pt^{2+}-O^{2-}$	2561.61	0.3200	0.00
$O^{2-}-O^{2-}$	9547.96	0.2192	32.00

Table 2. Shell Model Parameters

species	k/eV Å^2	Y/e
Ce^{4+}	177.84	−0.20
O^{2-}	6.3	−2.04

3. RESULTS

3.1. Characterization of Thin Film Electrodes. *3.1.1. Characterization by using XRD and RBS.* Thin film of CeO_x was fabricated on the Nb-STO SCS by using PLD method. To maximize the contact area of Pt−CeO_x interface on CeO_x thin film, we loaded a small amount of Pt on this CeO_x thin film.

Figure 1a shows the XRD pattern taken from Pt-loaded CeO_x film on $SrTiO_3$ (100) substrate. Only the (n00) reflections of CeO_2 and $SrTiO_3$ on $SrTiO_3$ (100) substrate were observed in this pattern. This result suggests that CeO_x thin film was epitaxially grown on $SrTiO_3$ (100) substrate in the present work. Because the observed Pt thickness (approximately 0.3 nm) was much less than the observed thickness of CeO_x film (approximately 50 nm), the thickness ratio of Pt (0.3

DOI: 10.1021/am507754w
ACS Appl. Mater. Interfaces 2015, 7, 2698−2707

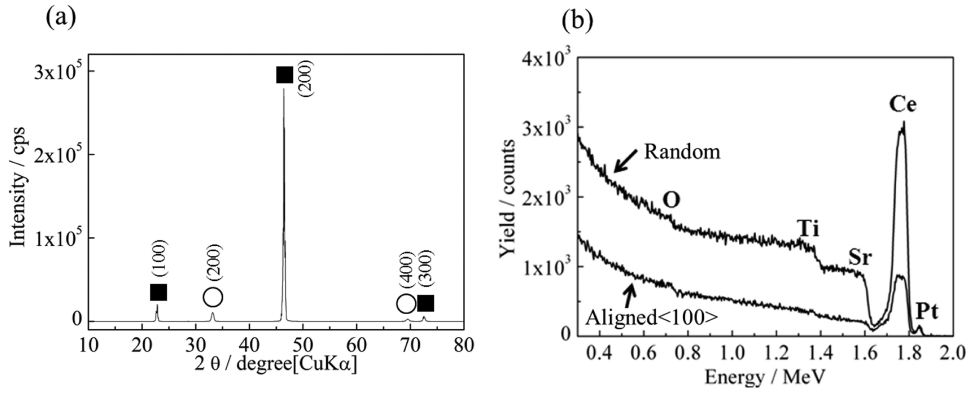

Figure 1. (a) X-ray diffraction pattern taken from Pt-loaded CeO_x thin film on Nb-doped $SrTiO_3$ single-crystal substrate; (○) CeO_2 and (■) $SrTiO_3$. (b) Rutherford backscattering spectrometry random spectra and aligned ⟨100⟩ spectra taken from Pt-loaded CeO_x thin film deposited on Nb-doped $SrTiO_3$ (100) single crystal substrate.

nm) to CeO_x (50 nm) was less than 4%, and it was under detectable level of XRD analysis in the present work.

To characterize the Pt-loaded CeO_x thin film which was grown on the substrate, we examined the crystallinity of the CeO_x thin film by using Rutherford backscattering spectrometry (RBS)/channeling analysis method as shown in Figure 1b. The spectra observed at 1.83, 1.73, and 0.72 MeV in Figure 1b correspond to the spectra of Pt, Ce, and O, respectively. The aligned spectrum was taken with the beam directed along the ⟨100⟩ axis of CeO_x film on the $SrTiO_3$ (100) substrate. Because the minimum yield (i.e., χ_{min}), which is the ratio between the random and the axially aligned yields, corresponds to the degree of crystallinity of the CeO_x thin film on the substrate, the χ_{min} value was estimated by using the observation result in Figure 1b. The χ_{min} value taken from Figure 1b was 0.32. It suggests that the epitaxial CeO_x film was grown on the Nb-STO SCS. Figure 1b also suggests that a small amount of Pt particles are observed on CeO_x thin film in the present work using RBS.

3.1.2. Surface Characterization by XPS. To compare the surface chemical states of previously reported Pt−CeO_x particle/C electrode and Pt-loaded CeO_x thin film on Nb-STO SCS, we examined the surface chemical states of Pt-loaded CeO_x thin film on the single crystal substrate by using SXPS. Also, the average surface chemical states of Pt-loaded CeO_x thin film sample were characterized by using HXPS, which has deeper probing depth as compared to SXPS. Figure 2 shows the Pt 4f spectra taken from Pt-loaded thin film electrodes by using SXPS and HXPS. As reference spectra, the Pt 4f spectra taken from both Pt-loaded on the single crystal substrate and Pt-loaded CeO_x thin film on the single-crystal substrate by using SXPS and HXPS are also shown in Figure 2. The Pt 4f spectra in Figure 2 show two spin−orbital splitting doublets Pt $4f_{7/2}$−$4f_{5/2}$. The peaks at 71.1 and 72.8 eV are attributed to metallic Pt (Pt^0) and divalent Pt (Pt^{2+}, PtO). The other extra peak at the binding energy of 72.1 eV which is labeled as Pt−X (X: O−Ce) would correspond to the slightly ionized Pt which is attributable to the formation of Pt−O−Ce bond at the interface between Pt and CeO_x.[17] Table 3 summarizes the content of metallic Pt and ionized Pt species taken from the surface of the thin film electrode by using SXPS and HXPS. In the previously reported Pt composition in Pt−CeO_x particle/C electrodes, the contents of Pt^{2+} and Pt−X (X: O−Ce) component on electrochemically pretreated sample with high ORR activity which were observed by SXPS was 3.8 and 8.9 at.

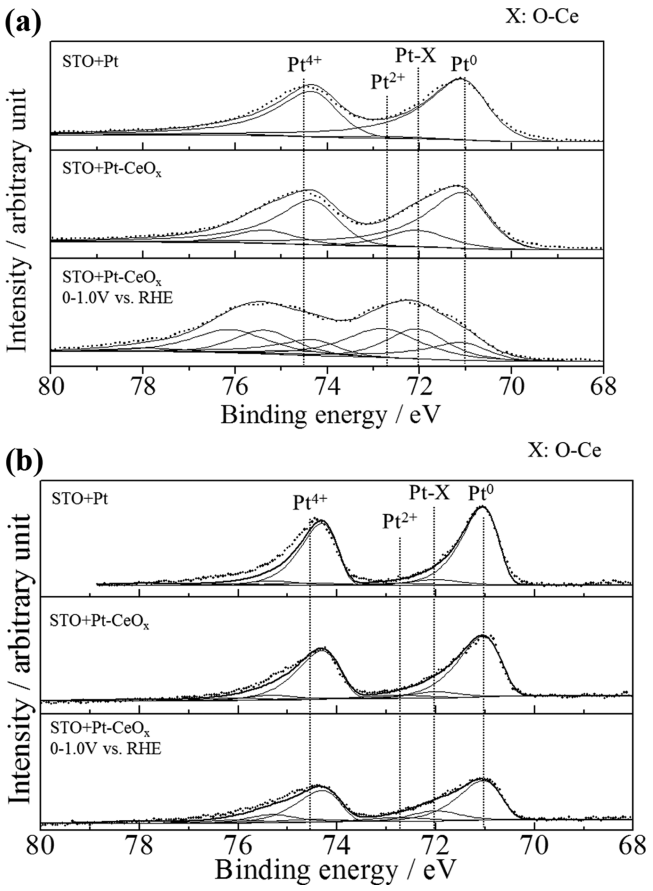

Figure 2. (a) Pt 4f spectra taken from Pt-loaded Nb-doped $SrTiO_3$ (100) substrate (STO + Pt), Pt-loaded CeO_x thin film on Nb-doped $SrTiO_3$ (100) substrate (STO + Pt−CeO_x), and electrochemically pretreated Pt-loaded CeO_x thin film on Nb-doped $SrTiO_3$ (100) substrate in potential ranging from 0 to 1.0 V (vs RHE) (STO + Pt−CeO_x, 0−1.0 V vs RHE) by using soft X-ray photoelectron spectroscopy. (b) Pt 4f spectra taken from Pt-loaded Nb-doped $SrTiO_3$(100) substrate (STO + Pt), Pt-loaded CeO_x thin film on Nb-doped $SrTiO_3$ (100) substrate (STO + Pt−CeO_x), and electrochemically pretreated Pt-loaded CeO_x thin film on Nb-doped $SrTiO_3$ (100) substrate in potential ranging from 0 to 1.0 V (vs RHE) (STO + Pt−CeO_x, 0−1.0 V vs RHE) by using hard X-ray photoelectron spectroscopy.

%, respectively. The average contents of Pt^{2+} and Pt−X (X: O−Ce) component on electrochemically pretreated sample with

DOI: 10.1021/am507754w
ACS Appl. Mater. Interfaces 2015, 7, 2698−2707

Table 3. Surface Analysis of Pt Species Using SXPS and HXPS

	SXPS analysis (at.%)			
samples	Pt^0	Pt−X	Pt^{2+}	Pt^{4+}
STO + Pt	95.6	0.5	3.5	0.4
STO + Pt−CeO_x	79.0	19.3	1.1	0.5
electrochemically pretreated STO + Pt−CeO_x	23.0	31.4	39.7	5.9
	HXPS analysis (at.%)			
samples	Pt^0	Pt−X	Pt^{2+}	Pt^{4+}
STO + Pt	84.5	7.8	3.1	4.6
STO + Pt−CeO_x	81.2	9.5	5.8	3.4
electrochemically pretreated STO + Pt−CeO_x	65.1	18.8	8.8	7.3

high ORR activity which were observed by HXPS were 7.9 and 17.4 at. %, respectively. SXPS and HXPS analysis data suggest that the surface of Pt was partially oxidized by formation of Pt−CeO_x interface in Pt-loaded CeO_x nanoparticles/C electrode. On the other hand, the average contents of Pt^{2+} and Pt−X (X: O−Ce) component on electrochemically pretreated Pt-loaded CeO_x thin film on conductive single crystal which were observed by HXPS were 8.8 and 18.8 at. % (Table 3), those observed values were almost same to that previously reported HXPS data of Pt−CeO_x particle/C.[16] Notice that the surface content of Pt cations (i.e., Pt^{2+} and Pt−X (X: O−Ce) species) on the electrochemically pretreated Pt-loaded CeO_x thin film on the conductive single crystal observed by SXPS was much higher than that on the previously reported electrochemically pretreated Pt-loaded CeO_x nanoparticle/C.[16] It indicates that the interaction between Pt and CeO_x can be promoted on the surface of CeO_x thin film. On the basis of the surface analysis data, we conclude that the interface between Pt and CeO_x is conspicuously formed on the CeO_x thin film, and the electrochemistry of Pt in Pt-loaded CeO_x thin film on Nb−STO SCS can be clearly observed in the present work.

Figure 3 presents the Ce 3d spectra taken from Pt-loaded CeO_x thin film on Nb−STO SCS, which were observed by using SXPS and HXPS. As reference spectra, the Ce 3d spectra taken from both the CeO_x thin film deposited on the single crystal substrate and the Pt-loaded CeO_x thin film deposited on the single-crystal substrate prior to the electrochemical pretreatment by using SXPS and HXPS are shown in Figure 3 as well. As shown in Figure 3, the components of Ce^{3+} (labeled by u_0, v_0, u′, v′, where the symbols u and v are spin−orbital partners of $3d_{5/2}$ and $3d_{3/2}$, respectively) and Ce^{4+}, which is labeled u, v, u′′, v″, u′′′ and v″′ in the figure (where the characters u and v are the aforementioned spin−orbital partners) were observed.

Table 4 summarizes the Ce^{3+}/Ce^{4+} ratio estimated from the surface of the thin film electrode by using SXPS and HXPS (see our detailed process of estimating the Ce^{3+}/Ce^{4+} ratio in the Supporting Information). The Ce 3d spectra, which we observed by using SXPS, are composed of Ce^{4+} and small amount Ce^{3+} species on the both reference samples (i.e., both of CeO_x thin film on the single-crystal substrate and Pt-loaded CeO_x thin film on the single crystal substrate prior to electrochemical pretreatment). The Ce^{3+}/Ce^{4+} ratio, which was estimated by using SXPS profiles, was approximately 0.13 in both cases. It suggested that Ce^{4+} was a major component on aforementioned two reference samples. After the electrochemical conditioning process, the free CeO_2, which has no interaction with Pt, would be resolved into H_2SO_4 aqueous solution, as reported in previous work.[16] As a result, the Ce^{3+}/Ce^{4+} ratio estimated from SXPS profile became approximately 1.36. It suggests that the Ce^{3+} which is stabilized into the CeO_x lattice by Pt−CeO_x interface formation is clearly observed on the surface of the Pt-loaded CeO_x on the substrate.

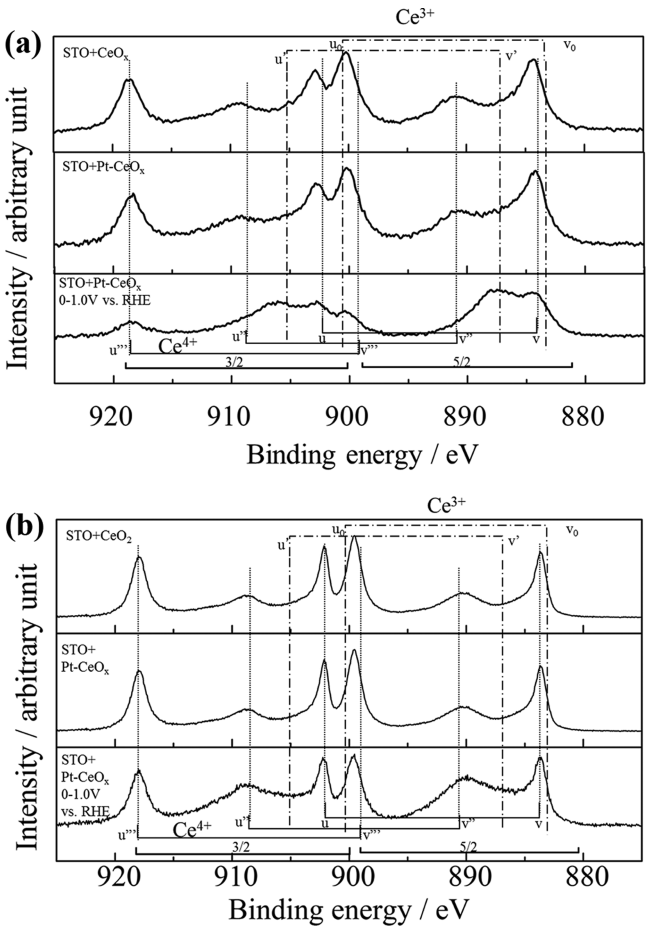

Figure 3. (a) Ce 3d spectra taken from CeO_x thin film on Nb-doped $SrTiO_3$ (100) substrate (STO + CeO_x), Pt-loaded CeO_x thin film on Nb-doped $SrTiO_3$ (100) substrate (STO + Pt−CeO_x), and electrochemically pretreated Pt-loaded CeO_x thin film on Nb-doped $SrTiO_3$ (100) substrate in potential ranging from 0 to 1.0 V (vs RHE) (STO + Pt−CeO_x, 0−1.0 V vs RHE) by using soft X-ray photoelectron spectroscopy. (b) Ce 3d spectra taken from CeO_x thin film on Nb-doped $SrTiO_3$ (100) substrate (STO + CeO_x), Pt-loaded CeO_x thin film on Nb-doped $SrTiO_3$ (100) substrate (STO + Pt−CeO_x), and electrochemically pretreated Pt-loaded CeO_x thin film on Nb-doped $SrTiO_3$ (100) substrate in potential ranging from 0 to 1.0 V (vs RHE) (STO+Pt−CeO_x, 0−1.0 V vs RHE) by using hard X-ray photoelectron spectroscopy.

DOI: 10.1021/am507754w
ACS Appl. Mater. Interfaces 2015, 7, 2698−2707

Table 4. Surface Analysis of Ce Species Using SXPS and HXPS

SXPS analysis	
samples	Ce^{3+}/Ce^{4+}
STO + Pt	
STO + Pt−CeO_x	0.13
electrochemically pretreated STO + Pt−CeO_x	1.36
HXPS analysis	
samples	Ce^{3+}/Ce^{4+}
STO + Pt	
STO + Pt−CeO_x	0.01
electrochemically pretreated STO + Pt−CeO_x	0.64

On the other hand, the Ce^{3+}/Ce^{4+} ratio estimated from the surface of the Pt-loaded CeO_x film on Nb-STO SCS by using HXPS after the electrochemical conditioning process was approximately 0.64. Even after taking into consideration the CeO_x surface reduction in the XPS measurement, the estimated Ce^{3+}/Ce^{4+} ratio after the electrochemical conditioning process as compared to Ce^{3+}/Ce^{4+} ratio which was estimated from the sample surface prior to the electrochemical conditioning process was conspicuously increased in the present analysis.

On the basis of the comparison of Ce^{3+}/Ce^{4+} ratios and content of Pt−X (X: O−Ce) species estimated from the electrochemically pretreated sample surfaces by using SXPS and HXPS, we concluded that the Pt−CeO_x interface was formed on the sample surface by interaction between Pt and CeO_x thin film surface and both Ce^{3+} and Pt−X (X: O−Ce) components which appeared on the Pt−CeO_x interface formation were clearly observed by using the XPS analyses (i.e., SXPS analysis and HXPS analysis).

In the previously reported surface analysis work for Pt−CeO_x particle/C electrodes, the Ce^{3+} was major component on the surface of electrochemically pretreated sample which was observed by using both SXPS and HXPS. The observed Ce 3d spectrum was quite weak and noisy as a result of small amounts of CeO_x which partially remained on the Pt electrode after the electrochemical pretreatment.[16] In contrast, we successfully observed clear Ce 3d spectra from the surface of electrochemically pretreated sample and estimated the aforementioned Ce^{3+}/Ce^{4+} ratios by using both SXPS and HXPS analyses. It suggests that the Pt-loaded CeO_x thin film on conductive Nb-STO SCS is useful for detail characterization of interface structure between Pt and CeO_x in Pt-loaded CeO_x electrodes.

After the surface characterization of Pt-loaded CeO_x thin film on the conductive Nb-STO SCS electrode, the electrochemical measurements were carried out by using Pt-loaded CeO_x thin film on Nb-STO SCS, and Pt-loaded Nb-STO SCS were observed in H_2SO_4 acidic aqueous solution.

3.2. Electrochemical Property Observed for Thin Film Electrode. As shown in Figure 4, the CV profile recorded from Pt-loaded Nb-STO SCS shows clear hydrogen adsorption and desorption peaks taken from Pt. It suggests that the reasonable electrochemical response is observed from Pt-loaded Nb-STO SCS in the present work. Note that the ohmic contact between the single-crystal substrate and the working electrode should be formed by using GaIn alloy paste for reliable measurement of electrochemistry. If the ohmic contact was not formed well, then we observed the electrochemistry of Nb-STO SCS instead of the electrochemistry of Pt surface. In that case, the observed

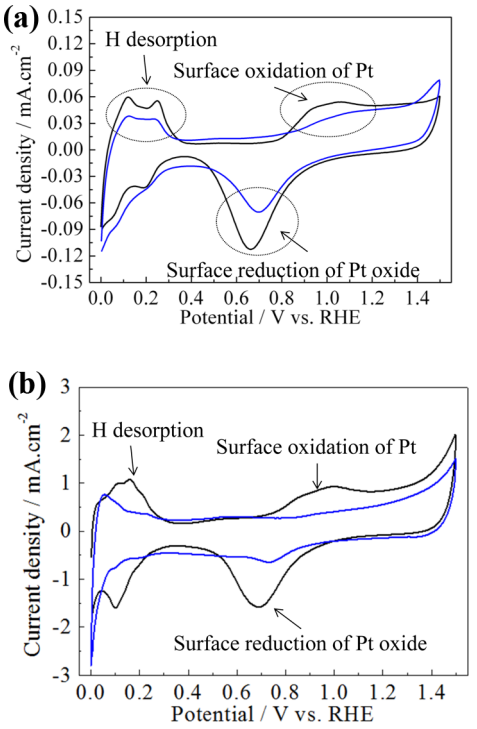

Figure 4. (a) Cyclic voltammograms recorded from (black) Pt loaded on $SrTiO_3$ (100) substrate and (blue) Pt-loaded CeO_x thin film on $SrTiO_3$ (100) substrate. Electrolyte, 0.5 M H_2SO_4 aqueous solution; measurement temperature, 28 °C; sweep rate, 50 mV sec^{-1}; cycle number, 30. Ohmic contact was made by using GaIn alloy paste. (b) Cyclic voltammograms recorded from (black) conventional Pt/C and (blue) Pt-loaded CeO_x nanoparticle/C. Electrolyte, 0.5 M H_2SO_4 aqueous solution; measurement temperature, 28 °C; sweep rate, 50 mV sec^{-1}; cycle number, 30.

current will be at μA cm^{-2} level or less, which is attributable to the n-type semiconducting property of Nb-STO SCS.

In general, the electrochemical response is assumed following electrochemical oxidation reactions on Pt.

$$Pt + H_2O \rightarrow Pt - OH + H^+ + e^- \quad (1)$$

$$Pt - OH \rightarrow Pt - O + H^+ + e^- \quad (2)$$

$$Pt - O + H_2O \rightarrow PtO_2 + 2H^+ + 2e^- \quad (3)$$

The oxidation level on Pt surface can be estimated by using the observed oxidation current as a ratio of oxidation charge (Q_{OX}) and hydrogen adsorption charge (Q_H). The OH adsorption on Pt (eq 1) proceeds from 0.80 to 1.08 V (vs RHE). The surface of Pt is fully covered with OH species. The charge ratio (i.e., $Q_{OX\ (0.80-1.08)}/Q_H$) is equal to 1. The OH species are gradually transformed into Pt−O species (eq 2) between 1.08 and 1.35 V (vs RHE). In this case, the charge ratio between Q_{OX} and Q_H (i.e., $Q_{OX(1.08-1.35)}/Q_H$) becomes 2. In the higher potential region, eq 3 would proceed to fabricate PtO_2 species.[27]

Table 5 summarizes the $Q_{OX(0.80-1.08)}/Q_H$ and $Q_{OX\ (1.08-1.35)}/Q_H$ ratios observed for Pt/C, Pt-loaded CeO_x particle/C, and Pt-loaded CeO_x on conductive Nb-STO SCS. Previously reported values are presented in Table 5 as a reference. The $Q_{OX(0.80-1.08)}/Q_H$ and $Q_{OX\ (1.08-1.35)}/Q_H$ ratios observed for Pt-loaded Nb-STO SCS were 0.98 and 2.02, respectively. Those observed charge ratios almost agreed with the previously reported ratio observed for the conventional Pt/C electrode.[25]

DOI: 10.1021/am507754w
ACS Appl. Mater. Interfaces 2015, 7, 2698−2707

Table 5. Comparison of Oxidation Level of Pt Surface Using Ratios of Oxidation Charge (Q_{OX}) and Hydrogen Adsorption Charge (Q_H)

samples	$Q_{OX}(1)/Q_H$[a]	$Q_{OX}(2)/Q_H$[a]	ref
Pt/C (powder)	1.0	2.0	27
Pt/C (powder)	0.7	1.9	
Pt−CeO_x particle/C	0.3	1.6	
Pt−CeO_xthin film/STO	0.3	1.3	

[a] Q_{OX}/Q_H = Q_{OX} (surface oxidation charge on Pt)/Q_H (H desorption charge from Pt surface). (1) and (2) indicate the potential measurement region: (1) from 0.80 to 1.08/V vs RHE and (2) from 1.08 to 1.35/V vs RHE.

In contrast, the $Q_{OX(0.80-1.08)}/Q_H$ and $Q_{OX(1.08-1.35)}/Q_H$ ratios observed for Pt-loaded CeO_x thin film on Nb-STO SCS were 0.3 and 1.3, respectively. Those observed charge ratios became smaller than Pt-loaded Nb-STO SCS. Also, the observed charge ratios on Pt-loaded CeO_x particles/C (i.e., $Q_{OX(0.80-1.08)}/Q_H$ ratio, 0.3; $Q_{OX\ (1.08-1.35)}/Q_H$ ratio, 1.6) were almost same as the Pt-loaded CeO_x thin film on Nb-STO SCS. These observations suggest that the surface oxidation of Pt in Pt-loaded CeO_x thin film deposited on the Nb-STO SCS electrode is suppressed by the formation of Pt−CeO_x interface on Pt and the previously reported Pt-loaded CeO_x nanoparticles/C electrode. Masuda et al.[19] examined the role of Pt−CeO_x interface on enhancement of surface activity of Pt by using in situ XAFS analysis technique. Their in situ X-ray absorption near edge structure (XANES) analysis indicated that the surface oxidation of Pt in Pt-loaded CeO_x nanoparticles/C was suppressed by the unique electrochemical redox reaction of CeO_x (i.e., $Ce^{3+} \leftrightarrow Ce^{4+}$) in the Pt−$CeO_x$ interface at room temperature. The CV observed for the surface of Pt-loaded CeO_x thin film on the Nb-STO SCS electrode in Figure 4 clearly reproduced the effect of Pt−CeO_x interface formation on suppression of surface oxidation of Pt in Pt−CeO_x particles/C.

3.3. Microstructure Characterization by TEM. To clarify the Pt−CeO_x interface structure on Pt, we observed the crystal structural feature in the cross section of Pt-loaded CeO_x thin film on Nb-STO SCS using TEM. Before the observation of cross section of Pt-loaded CeO_x thin film on Nb-STO SCS, the crystal orientation between epitaxial growth CeO_x thin film and Nb-STO SCS was concluded, as shown in Figure 5. Figure 5a shows that the CeO_x thin film grown along (100) direction on Nb-STO SCS has the same crystal orientation in the top view. On the other hand, the CeO_x thin film grown on $SrTiO_3$ (010) single crystal shows the (011) direction to minimize the misfit of crystal orientation between CeO_x thin film and single crystal substrate (see side view image in Figure 5b).

On the basis of this conclusion about the crystal orientation between epitaxial growth CeO_x thin film and Nb-STO SCS, we performed TEM image observation on cross sections of the sample cut from Pt-loaded CeO_x thin film on Nb-STO SCS. Figure 6a presents the high-resolution image taken from the cross section of Pt-loaded CeO_x thin film on Nb-STO SCS. The figure clearly shows the complexity of the microstructure at the nanoscale. The nature of the sample is such that it is not uniform on the nanoscale. If this were a perfect crystal, then the microscopy would be greatly simplified. However, this material has been modified, and the nature of these CeO_x-based systems is that there are domains and localized defects that will impart some distortion of the lattice, which is our reason for showing this micrograph. To clarify the representative feature of microstructure, we present the fast Fourier transforms (FFT) patterns (Figure 6b) that correspond to the microscopic area in Figure 6a.

The FFT pattern (i.e., (1−2) in Figure 6b) taken from the TEM image of area (1−1) in Figure 6a corresponds to the typical electron diffraction pattern recorded from $SrTiO_3$ (010) substrate. Also, the FFT pattern (i.e., (2−2) in Figure 6b) taken from area (2−1) in Figure 6a shows typical electron diffraction pattern of cerium oxide with fluorite structure. In contrast, the extra reflections were observed in the FFT pattern (i.e., (3−2) in Figure 6b) which was taken from area (3−1) in Figure 6a. All reflections in (3−2) in Figure 6b agreed with the reflections of C-type rare earth structure. The inverse FFT patterns taken from (2−2) and (3−2) of Figure 6b show the different fringe contrast images, as shown in (2−3) and (3−3) of Figure 6c. We concluded that the fringe contrasts (2−3) and (3−3) of Figure 6c corresponds to the crystal structural feature of fluorite structure and C type rare earth structure, respectively.

Microanalysis results in Figure 6 suggest that the heterointerface between Pt and CeO_x, which was created by dissolution of Pt cation into fluorite CeO_x lattice, promotes the charge transfer phenomena between Pt electrode and CeO_x at nanoscale. Also, this active charge transfer promotes the electrochemical redox reaction of CeO_x (i.e., $Ce^{3+} \leftrightarrow Ce^{4+}$)

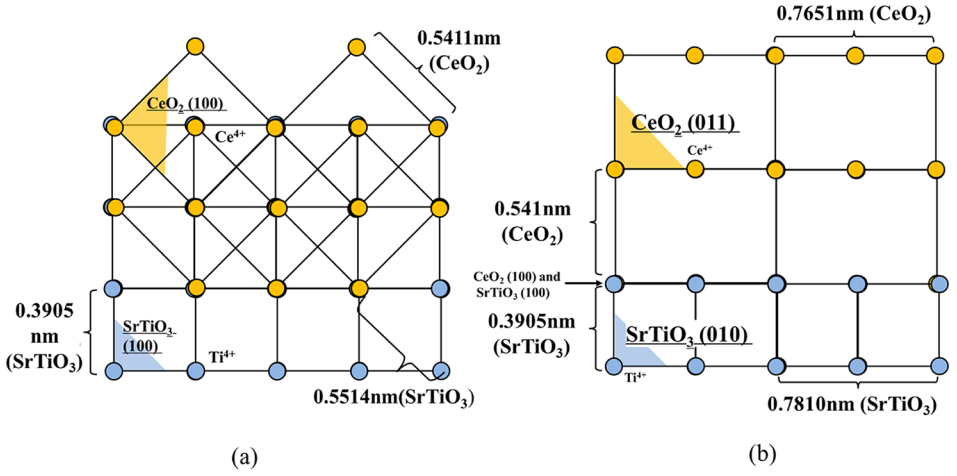

Figure 5. Expected crystal orientation of CeO_x thin film deposited on conductive $SrTiO_3$ (100) substrate (100) from (a) top view and (b) side view.

DOI: 10.1021/am507754w
ACS Appl. Mater. Interfaces 2015, 7, 2698−2707

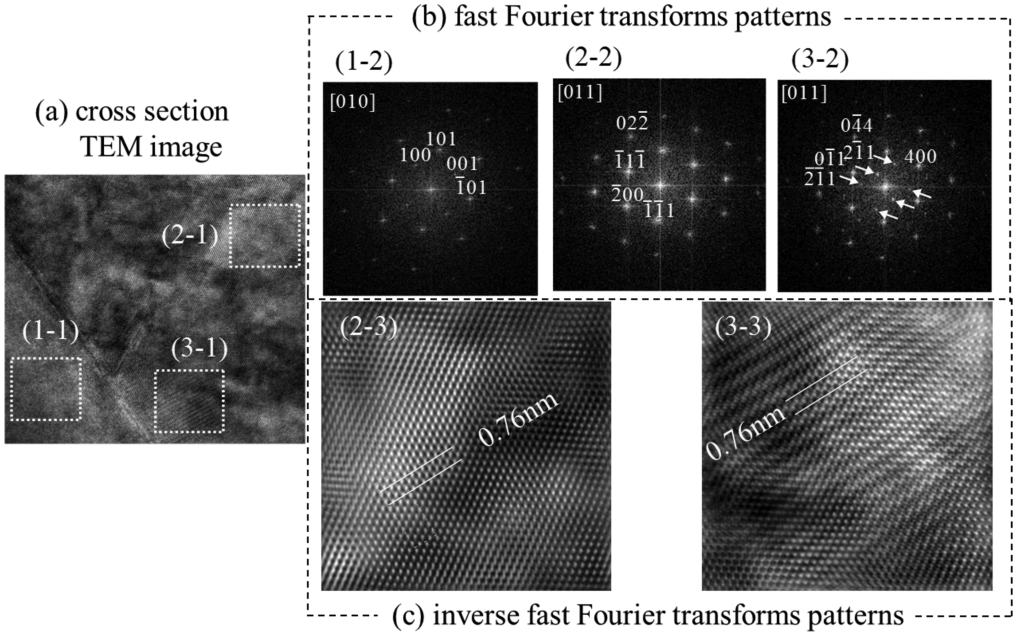

Figure 6. (a) TEM cross-sectional image taken from electrochemically pretreated Pt-loaded CeO_x thin film on conductive Nb-doped $SrTiO_3$ (100) single crystal substrate. (b) Fast Fourier transforms patterns: (1−2) transformed from 1 to 1, (2−2) transformed from 2 to 1, and (3−2) transformed from 3 to 1. (c) Inverse fast Fourier transforms patterns: (2−3) transformed from 2 to 2 and (3−3) transformed from 3 to 2.

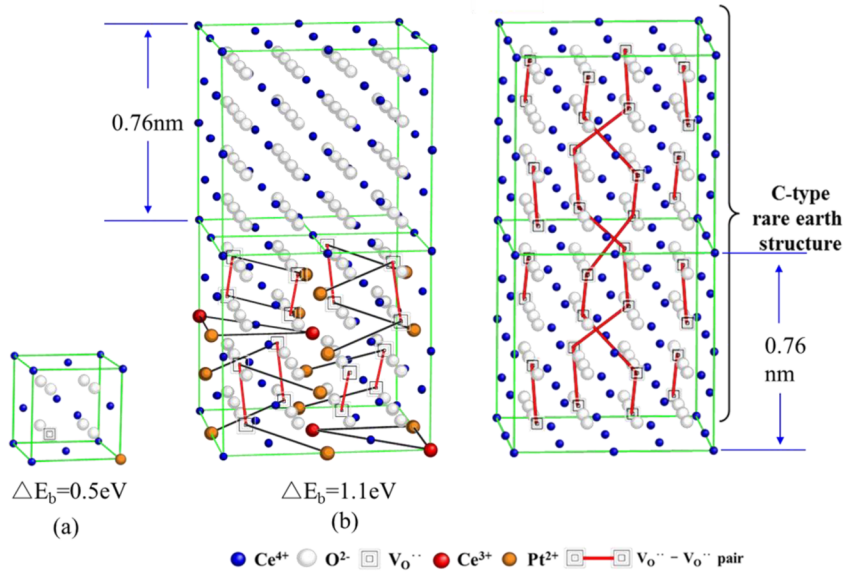

Figure 7. Calculated biding energy (ΔE_b) and defect structure model based on (a) $Pt_{Ce}''-Vo^{\bullet\bullet}$ cluster and (b) 12 ($Pt_{Ce}''-Vo^{\bullet\bullet}$) + 2 ($Pt_{Ce}''-2Vo^{\bullet\bullet}-2Ce_{Ce}'$) cluster. The defect structure of the C-type rare earth structure was displayed as reference.

in the Pt−CeO_x interface at room temperature. Consequently, the Pt surface oxidation would be effectively suppressed by the electrochemical redox reaction of CeO_x in the Pt−CeO_x heterointerface on Pt electrode as shown in Figure 4.

4. DISCUSSION

On the basis of the results of electrochemistry observed for Pt-loaded CeO_x thin film electrode grown on the Nb-STO SCS and the microanalysis of the cross-sectional TEM image taken of the thin film electrode, we concluded that the Pt−CeO_x heterointerface on Pt plays a key role in maximizing the CeO_x promotion effect on Pt. To interpret the microanalysis results of Pt−CeO_x heterointerface well and develop the design concept of Pt−CeO_x heterointerface, we performed the atomistic simulation of Pt−CeO_x heterointerface on Pt using interatomic potential and shell model.[26]

XPS analysis results observed for Pt−CeO_x thin film on the conductive single crystal (Figure 3) and Pt−CeO_x particle/C cathode[16] suggest that the Pt−CeO_x interface on Pt mainly consists of Pt^{2+} and Ce^{3+} species. On the basis of those results, we can assume the dissolution of Pt into CeO_x lattice in the Pt−CeO_x interface through the following empirical reaction:

$$Pt + 2Ce^{x}_{Ce} \xrightarrow{CeO_2} Pt''_{Ce} + 2V_o^{\cdot\cdot} + 2Ce_{Ce}' \quad (4)$$

where the Kröger-Vink notation is used for explanation of solid solution creation and defect structure formation. According to

DOI: 10.1021/am507754w
ACS Appl. Mater. Interfaces 2015, 7, 2698−2707

this defect formation equation, Ce^{4+} cations need to be reduced to Ce^{3+} at the Pt−CeO_x interface for the balance of local oxygen vacancy concentration. Based on this assumption, the stable configuration of the Pt_{Ce}''−$Vo^{\bullet\bullet}$ cluster in the unite cell of fluorite-type structure CeO_2 can be estimated by using the atomistic simulation. If the binding energy (E_b) of the defect cluster was the highest level in all other configurations in the unit cell, the present atomistic simulation work predicts that the configuration of defect cluster with the highest E_b is stable enough in the unit cell.

The highest binding energy of Pt_{Ce}''−$Vo^{\bullet\bullet}$ cluster in all possible configurations in the unit cell was E_b = 0.5 eV. Figure 7a demonstrates the stable configuration of Pt_{Ce}''−$Vo^{\bullet\bullet}$ cluster with the highest E_b. Alternatively, other candidate of stable configuration based on the defect formation eq 4 is Pt_{Ce}''−$2Vo^{\bullet\bullet}$−$2Ce_{Ce}'$ cluster. However, the binding energy calculation based on the defect configuration in eq 4 was negative, suggesting that the formation of this cluster is unstable. To explore more stable and larger clusters in the Pt−CeO_x interface, we built the large clusters by combining the Pt_{Ce}''−$Vo^{\bullet\bullet}$ and Pt_{Ce}''−$2Vo^{\bullet\bullet}$−$2Ce_{Ce}'$ structures based on the C-type rare earth structure, which is thermodynamically stable with fluorite structure in one phase diagram, as shown in eq 5 and Figure 7b.

$$12(Pt_{Ce}'' - Vo^{\cdot\cdot}) + 2(Pt_{Ce}'' - 2Vo^{\cdot\cdot} - 2Ce_{Ce}') \rightarrow \text{C-type rare earth like defect structure} \quad (5)$$

The calculated E_b based on eq 5 was 1.1 eV which was conspicuously higher than the E_b value based on the smallest cluster model (i.e., Pt_{Ce}''−$Vo^{\bullet\bullet}$). The present atomistic simulation results clearly indicate that Pt cations have diffused into the CeO_x lattice from the Pt surface and dissolved into the CeO_2 fluorite lattice to make a stable large defect clusters in Pt−CeO_x interface. Also, the large defect structure consisted of C-type rare-earth-like structure, which is a fluorite-related structure. In the electrochemistry reaction, when potential was applied to the surface of Pt with Pt−CeO_x interface, the electron migration from the active metal Pt surface to CeO_x would be promoted by the unique Pt−CeO_x interface. Then, the electrochemical redox reaction of CeO_x at room temperature, which was suggested by Masuda et al.,[19] was produced under the applied potential for measurement of the electrode reaction. In addition, it is concluded that the charge transfer from CeO_x to Pt under the applied potential pushes the Fermi level of Pt up, and the electrons of the Pt surface move to the lowest unoccupied molecular orbital (LUMO) of the oxygen which adsorbed on the Pt surface. Finally, the ORR activity on Pt is improved by the promotion effect of CeO_x in Pt−CeO_x heterointerface, as shown in the WGS reaction on Pt−CeO_x catalyst surface by Bruix et al.[22] and in the CO oxidation reaction on Pt−CeO_x catalyst surface by Suchorski et al.[23]

Because the atomic coordinates of Pt−CeO_x interface structure model was refined on the basis of present atomistic simulation results, in the next step of the present work, the electron energy loss spectroscopy (EELS) profiles such as O K-edge and Ce M-edge will be calculated using theoretical calculation. Through this challenge, we expect to optimize the Pt−CeO_x interface structure by comparison between the calculated EELS profiles and observed ones for the sample with optimized interface structure in order to maximize the ORR property on Pt and minimize the Pt content in the electro-catalyst for fuel cell application. In this future challenge, the mechanism of spillover from platinum to CeO_x on CeO_x/Cu(111) reported by Wrobel et al.[28] and the impact of impurity such as sulfur on the redox property of CeO_x, which was previously reported by Wrobel and Becker,[29] should be considered, as well as the optimization of the Pt−CeO_x defect interface structure. Through the aforementioned works, high-quality electro-catalyst will be developed as a practical solution for fuel cell application.

5. CONCLUSIONS

Pt-loaded CeO_x thin film on the conductive Nb-STO SCS electrode fabricated by a stepwise process of pulse laser deposition for CeO_x thin film and impregnation of Pt particle loading on CeO_x thin film. Microanalysis of the cross-sectional image of the Pt−CeO_x thin film was performed by TEM. Our combination analysis of microanalysis and atomistic simulation based on the microanalysis results indicate that C-type rare-earth-like structure comprising unique, large defect clusters 12 (Pt_{Ce}''−$Vo^{\bullet\bullet}$) + 2 (Pt_{Ce}''−$2Vo^{\bullet\bullet}$−$2Ce_{Ce}'$) were formed in Pt−CeO_x interface. These large defect clusters, which were formed by strong interaction between Pt and CeO_x, could promote charge transfer between the surface of Pt electrode and CeO_x lattice in the Pt−CeO_x interface. This process can consequently suppress the surface oxidation of the Pt electrode and may enhance the performance of Pt, as previously reported. Accordingly, the evolution of C-type rare-earth-like structure in Pt−CeO_x interface should not be neglected and could maximize the ORR activity on Pt by maximizing the large defect cluster population in the interface between Pt and CeO_x.

■ ASSOCIATED CONTENT

Ⓢ Supporting Information

Analysis procedure for determination of Ce^{3+}/Ce^{4+} ratio. This material is available free of charge via the Internet at http://pubs.acs.org.

■ AUTHOR INFORMATION

Corresponding Author

*E-mail: MORI.Toshiyuki@nims.go.jp. Tel.: +81-29-860-4395. Fax: +81-29-860-4712.

Notes

The authors declare no competing financial interest.

■ ACKNOWLEDGMENTS

Partial financial support from the Grant-in-Aid for Scientific Research B (No.25281066) by the Ministry of Education, Culture, Sports, and Technology (MEXT), Japan, is gratefully acknowledged. Also, the authors appreciate the partial funding support from the Global Research Center for Environmental and Energy based on Nanomaterials Science (GREEN), National Institute for Materials Science (NIMS), Japan.

■ REFERENCES

(1) Springer, T. E.; Zowodzinski, T. A.; Gottesfeld, S. Polymer Electrolyte Fuel Cell Model. *J. Electrochem. Soc.* **1991**, *138*, 2334−2342.

(2) Kordesch, K. V.; Simader, G. R. Environmental Impact of Fuel Cell Technology. *Chem. Rev.* **1995**, *95*, 191−207.

(3) Steele, B. C. H.; Heinzel, A. Materials for Fuel-Cell Technologies. *Nature* **2001**, *414*, 345−352.

(4) Gong, K.; Du, F.; Xia, Z.; Durstock, M.; Dai, L. Nitrogen-Doped Carbon Nanotube Arrays with High Electrocatalytic Activity for Oxygen Reduction. *Science* **2009**, *323*, 760−764.

DOI: 10.1021/am507754w
ACS Appl. Mater. Interfaces 2015, 7, 2698−2707

(5) Qu, L.; Liu, Y.; Baek, J.-B.; Dai, L. Nitrogen-Doped Graphene as Efficient Metal-Free Electro-catalyst for Oxygen Reduction in Fuel Cells. *ACS Nano* **2010**, *4*, 1321−1326.
(6) Yang, S.; Feng, X.; Wang, X.; Mullen, K. Graphene-based Carbon Nitride Nanosheets as Efficient Metal-Free Electrocatalysts for Oxygen Reduction Reactions. *Angew. Chem., Int. Ed. Engl.* **2011**, *50*, 5339−5343.
(7) Yang, Z.; Yao, Z.; Li, G.; Fang, G.; Nie, H.; Liu, Z.; Zhou, X.; Chen, X.; Huang, S. Sulfur-Doped Graphene as an Efficient Metal-Free Cathode Catalyst for Oxygen Reduction. *ACS Nano* **2012**, *6*, 205−211.
(8) Zhang, Y. J.; Fugane, K.; Mori, T.; Niu, L.; Ye, J. Wet Chemical Synthesis of Nitrogen-Doped Graphene towards Oxygen Reduction Electrocatalysts without High-Temperature Pyrolysis. *J. Mater. Chem.* **2012**, *22*, 6575−6580.
(9) Shim, J.; Lee, C.-R.; Lee, H.-K.; Lee, J.-S.; Cairns, E. J. Electrochemical Characteristics of Pt-WO_3/C and Pt-TiO_2/C Electrocatalysts in a Polymer Electrolyte Fuel Cell. *J. Power Sources* **2001**, *102*, 172−177.
(10) Sasaki, K.; Zhang, L.; Adzic, R. R. Niobium Oxide-Supported Platinum Ultra-low Amount Electrocatalysts for Oxygen Reduction. *Phys. Chem. Chem. Phys.* **2008**, *10*, 159−167.
(11) Parrondo, J.; Mijangos, F.; Rambabu, B. Platinum/Tin Oxide/Carbon Cathode Catalyst for High-Temperature PEM Fuel Cell. *J. Power Sources* **2010**, *195*, 3977−3983.
(12) Takahashi, M.; Mori, T.; Ye, F.; Vinu, A.; Kobayashi, H.; Drennan, J. Design of High-Quality Pt−CeO_2 Composite Anodes Supported by Carbon Black for Direct Methanol Fuel Cell Application. *J. Am. Ceram. Soc.* **2007**, *90*, 1291−1294.
(13) Takahashi, M.; Mori, T.; Yoshikawa, H.; Togasaki, K.; Fugane, A.; Tada, A.; Matolin, V.; Drennan, J. Influence of Pt and CeO_2 Interaction in Pt−CeO_2 Electrode on Anode and Cathode Performance for Fuel Cell Applications. *Trans. Mater. Res. Soc. Jpn.* **2008**, *33*, 1101−1104.
(14) Lim, D.-H.; Lee, W.-D.; Choi, D.-H.; Kwon, H.-H.; Lee, H.-I. The Effect of Cerium Oxide Nanoparticles on a Pt/C Electrocatalyst Synthesized by a Continuous Two-Step Process for Low-Temperature Fuel Cell. *Electrochem. Commun.* **2008**, *10*, 592−596.
(15) Lim, D.-H.; Lee, W.-D.; Choi, D.-H.; Lee, H.-I. Effect of Ceria Nanoparticles into the Pt/C Catalyst as Cathode Material on the Electrocatalytic Activity and Durability for Low-Temperature Fuel Cell. *Appl. Catal,. B* **2010**, *94*, 85−96.
(16) Fugane, K.; Mori, T.; Ou, D. R.; Suzuki, A.; Yoshikawa, H.; Masuda, T.; Uosaki, K.; Yamashita, Y.; Ueda, S.; Kobayashi, K.; Okazaki, N.; Matolinova, I.; Matolin, V. Activity of Oxygen Reduction Reaction on Small Amount of Amorphous CeO_x Promoted Pt Cathode for Fuel Cell Application. *Electrochim. Acta* **2011**, *56*, 3874−3883.
(17) Fugane, K.; Mori, T.; Ou, D. R.; Yan, P. F.; Yoshikawa, H.; Drennan, J. Improvement of Cathode Performance on Pt−CeO_x by Optimization of Electrochemical Pretreatment Condition for PEFC Application. *Langmuir* **2012**, *28*, 16692−16700.
(18) Mori, T.; Ou, D. R.; Zou, J.; Drennan, J. Present Status and Future Prospect of Design of Pt−Cerium Oxide Electrodes for Fuel Cell Applications. *Prog. Nat. Sci.: Mater. Int.* **2012**, *22*, 561−571.
(19) Masuda, T.; Fukumitsu, H.; Fugane, K.; Togasaki, H.; Matsumura, D.; Tamura, K.; Nishihata, Y.; Yoshikawa, H.; Kobayashi, K.; Mori, T.; Uosaki, K. Role of Cerium Oxide in the Enhancement of Activity for the Oxygen Reduction Reaction at Pt−CeO_x Nanocomposite Electrocatalyst—An in Situ Electrochemical X-ray Absorption Fine Structure Study. *J. Phys. Chem. C* **2012**, *116*, 10098−10102.
(20) Ou, D. R.; Mori, T.; Togasaki, H.; Takahashi, M.; Ye, F.; Drennan, J. Microstructural and Metal-support Interactions of the Pt−CeO_2/C Catalysts for Direct Methanol Fuel Cell Application. *Langmuir* **2011**, *27*, 3859−3866.
(21) Ou, D. R.; Mori, T.; Fugane, K.; Togasaki, H.; Ye, F.; Drennan, J. Stability of Ceria Supports in Pt−CeO_x/C Catalysts. *J. Phys. Chem. C* **2011**, *115*, 19239−19245.
(22) Bruix, A.; Rodriguez, J. A.; Ramirez, P. J.; Senanayake, S. D.; Evans, J.; Park, J. B.; Stacchiola, D.; Liu, P.; Hrbek, J.; Illas, F. A New Type of Strong Metal−Support Interaction and the Production of H_2 through the Transformation of Water on Pt/CeO_2(111) and Pt/CeO_2/TiO_2(110) Catalysts. *J. Am. Chem. Soc.* **2012**, *134*, 8968−8974.
(23) Suchorski, Y.; Wrobel, R.; Becker, S.; Strzelczyk, B.; Drachsel, W.; Weiss, H. Ceria Nanoformations in CO Oxidation on Pt(111): Promotion Effects and Reversible Redox Behavior Surface. *Surf. Sci.* **2007**, *601*, 4843−4848.
(24) Yamamoto, S.; Sumita, T.; Sugiharuto; Miyashita, A.; Naramoto, H. Preparation of Epitaxial TiO_2 Films by Pulsed Laser Deposition Technique. *Thin Solid Films* **2001**, *401*, 88−93.
(25) Ma, J. L.; Ye, F.; Ou, D. R.; Li, L. L.; Mori, T. Structures of Defect Clusters on Ceria {111} Surface. *J. Phys. Chem. C* **2012**, *116*, 25777−25782.
(26) Gale, J. D. GULP: A Computer Program for the Symmetry-Adapted Simulation of Solids. *J. Chem. Soc., Faraday Trans.* **1997**, *93*, 629−637.
(27) Imai, H.; Izumi, K.; Matsumoto, M.; Kubo, Y.; Kato, K.; Imai, Y. In Situ and Real-Time Monitoring of Oxide Growth in a Few Monolayers at Surfaces of Platinum Nanoparticles in Aqueous Media. *J. Am. Chem. Soc.* **2009**, *131*, 6293−6300.
(28) Wrobel, R.; Suchorski, Y.; Becker, S.; Weiss, H. Cerium Oxide Layers on the Cu(111) Surface: Substrate-Mediated Redox Properties. *Surf. Sci.* **2008**, *602*, 436−442.
(29) Wrobel, R. J.; Becker, S. Carbon and Sulphur on Pd(111) and Pt(111): Experimental Problems during Cleaning of the Substrates and Impact of Sulphur on the Redox Properties of CeO_x in the CeO_x/Pd(111) System. *Vacuum* **2010**, *84*, 1258−1265.

DOI: 10.1021/am507754w
ACS Appl. Mater. Interfaces 2015, 7, 2698−2707